POLITECNICO DI TORINO
Repository ISTITUZIONALE

Design and testing of BACCOs, a gravity-compensated robotic manipulator for wine sampling

Original
Design and testing of BACCOs, a gravity-compensated robotic manipulator for wine sampling / Tagliavini, L., Botta, A., Pacheco Quinones, D., Quaglia, G., Maffiodo, D.. - In: INDUSTRIAL ROBOT. - ISSN 0143-991X. - (2026), pp. 1-13. [10.1108/IR-03-2026-0135]

Availability:
This version is available at: 11583/3016334 since: 2026-10-05T13:13:16Z

Publisher:
Emerald Publishing

Published
DOI:10.1108/IR-03-2026-0135

Terms of use:

This article is made available under terms and conditions as specified in the corresponding bibliographic description in the repository

Publisher copyright

(Article begins on next page)

26 October 2026

Design and testing of BACCOs, a gravity-compensated robotic manipulator for wine sampling

Luigi Tagliavini, Andrea Botta, Daniel Pacheco Quinones, Giuseppe Quaglia and Daniela Maffiodo
Department of Mechanical and Aerospace Engineering (DIMEAS), Politecnico di Torino, Turin, Italy

Abstract

Purpose – This paper aims to present the design, modeling and experimental validation of Automatic Collection and Conveyance of Oenologic Samples (BACCOs), a low-degree-of-freedom (DOF), gravity-compensated robotic manipulator for automated wine sampling. This study focuses on the mechanical design of a four-DOF robotic arm, intended to be mounted on a two-DOF mobile platform to perform autonomous sampling operations.

Design/methodology/approach – To meet the specific requirements of the application, the robotic arm design incorporates a planar double-parallelogram mechanism for end-effector positioning, along with two additional joints to compensate for pose errors of the mobile base. Two independent passive gravity-compensation systems, namely, a spring-wire system and a spring-wire-cam system, are implemented to enable energy-efficient operation of the double-parallelogram mechanism and the use of low-power actuators.

Findings – The robotic arm has been built and experimentally tested in a laboratory environment, demonstrating the effectiveness of the gravity-balancing systems.

Originality/value – The proposed design satisfies the key application requirements, particularly the need for a large workspace (in fact, barrel taps are typically located between 1.1 and 1.81 m above floor level and within corridors up to 2 m wide), while ensuring a lightweight and energy-efficient solution. Moreover, the paper presents a modified graphical method for the design of the cam used in one of the gravity-compensation systems, building on previous literature on cam design.

Keywords Mobile manipulators, Robot design, Passive gravity compensation, Cam design, Energy efficiency

Paper type Research paper

1. Introduction

Winemaking has ancient origins. Archaeologists suggest that the practice of collecting grapes to produce fermented beverages dates back as early as 8,000 BC in the Transcaucasus (Millon, 2013). In 2011, a group of archaeologists published the paper (Barnard *et al.*, 2011) reporting the discovery of chemical evidence for wine production around 4,000 BCE in Armenia. They found a wine press for stomping grapes, fermentation and storage vessels, drinking cups and withered grape vines, skins and seeds. Over the years, the winemaking process has evolved, incorporating new techniques and technologies while maintaining regional traditions and characteristics.

In summary, the winemaking process can be structured in the following steps: grape harvest, destemming and crushing, fermentation, racking and pressing, malolactic fermentation, refining or aging, bottling and storage. During the winemaking process, wine is monitored at various stages to ensure its quality, consistency and safety. The monitoring takes place from the moment the grapes are harvested until the wine is bottled and ready for consumption. The key processes that require special monitoring are alcoholic fermentation and maturation, in which malolactic fermentation occurs. Chemical and physical analyses are performed in a laboratory to monitor the wine during these phases.

Mobile manipulators are designed to perform complex tasks that require both manipulation and navigation in dynamic environments. These systems typically combine a robotic arm with a mobile base, enabling them to interact with objects and move through diverse terrains (Siegwart *et al.*, 2011; Kececi and Ceccarelli, 2015). Recent advances focus on improving autonomy (Arvin *et al.*, 2018), ground adaptability (Watanabe *et al.*, 2024) and precision through the integration of advanced control algorithms and actuation, as well as artificial intelligence (Hong *et al.*, 2024) and machine learning algorithms (Xiao *et al.*, 2022). Applications range from industrial automation,

The current issue and full text archive of this journal is available on Emerald Insight at: **https://www.emerald.com/insight/0143-991X.htm**

Industrial Robot: the international journal of robotics research and application
Emerald Publishing Limited [ISSN 0143-991X]
[DOI 10.1108/IR-03-2026-0135]

© Luigi Tagliavini, Andrea Botta, Daniel Pacheco Quinones, Giuseppe Quaglia and Daniela Maffiodo. Published by Emerald Publishing Limited. This article is published under the Creative Commons Attribution (CC BY 4.0) licence. Anyone may reproduce, distribute, translate and create derivative works of this article (for both commercial and non-commercial purposes), subject to full attribution to the original publication and authors. The full terms of this licence may be seen at http://creativecommons.org/licences/by/4.0/

Funding: This paper is part of the project NODES which has received funding from the MUR – M4C2 1.5 of PNRR funded by the European Union – NextGenerationEU (Grant agreement no. ECS00000036).

Received 19 March 2026
Revised 31 July 2026
31 August 2026
Accepted 4 September 2026

Downloaded from www.emerald.com/ir/article-pdf/doi/10.1108/IR-03-2026-0135/11890658/ir-03-2026-0135en.pdf by Politecnico di Torino user on 05 October 2026

such as logistics and manufacturing (Fragapane *et al.*, 2021), to service robotics in agriculture (Colucci *et al.*, 2022; Quaglia *et al.*, 2022), as well as in health care (Gacovski and Gacovski, 2011) and adverse terrain exploration (Pao *et al.*, 2022). Researchers are tackling challenges such as real-time perception (Jokić *et al.*, 2022), efficient navigation (Payá *et al.*, 2020), human–robot collaboration (Chen *et al.*, 2023) and weight balancing.

Given the specific application of automatic wine sampling, the size of the system under analysis is expected to be considerable because the barrel taps are mounted between 1.1 and 1.8 m above the ground. During wine-sampling operations, the end effector remains stationary and is then retracted before moving to the next barrel. Given this type of use, a gravity compensation system can significantly enhance the energy efficiency of the robotic arm, because otherwise the actuators would be primarily used to maintain a fixed configuration. Passive weight compensation approaches allow mobile robots to extend operational time, making them more efficient in applications where battery life is a critical factor.

Gravity compensation systems have been widely studied since the 1980s to reduce the energy consumption caused by gravity acting on the masses of the manipulator links. Energy consumption is particularly relevant in mobile manipulators, where a decrease in energy consumption results in improved overall autonomy. Two methods are adopted in conventional passive balancing systems (Yin, 2014; Arakelian, 2016; Endo *et al.*, 2010), mainly: mass balance by means of counterweights (Lowen *et al.*, 1983) and elastic balance by means of springs (Herder, 2001; Te Riele and Herder, 2001; Mashayekhi *et al.*, 2014). Counterweights are added to keep the center of mass of moving links stationary. Their effectiveness is well known, but they increase the total mass, overall size of the robot and the joint effort required for fast motions (Arakelian, 2016). The gravity compensation can also be achieved using springs attached directly to the robot links or using cables and pulley arrangements. Based on the torque profile that needs to be balanced, the spring properties and attachment points are evaluated. Particular attention must be devoted to zero-free-length and non-zero-free-length springs (Arakelian, 2016; Endo *et al.*, 2010) because of their effect on gravity compensation results. In those cases where more parameters are needed to achieve gravity compensation, the adoption of noncircular pulleys on which the cables attached to the springs wrap around has been proposed in the literature (Endo *et al.*, 2010; Kilic *et al.*, 2012).

In this context, this paper proposes the design of a low-mobility, gravity-compensated robot for Automatic Collection and Conveyance of Oenologic Samples (BACCOs). Previous research has already explored the development of a wine collection system equipped with cleaning routines between samples to prevent cross-contamination. The objective of this work is to design a low-mobility robotic arm capable of positioning this custom sampling device at the extraction point on the wine reservoir. The proposed manipulator is intended to be mounted on an autonomous mobile platform, as schematically illustrated in Figure 1. The main contributions of this work are summarized in the following bulleted list:

- functional design of a custom low-mobility robotic arm to perform the specific and peculiar wine-sampling activities in industrial wine cellars;

Figure 1 BACCOs concept and reference frames definition: $\{b\}$ base platform reference frame, $\{0\}$ BACCOs base reference frame and $\{EE\}$ end-effector reference frame

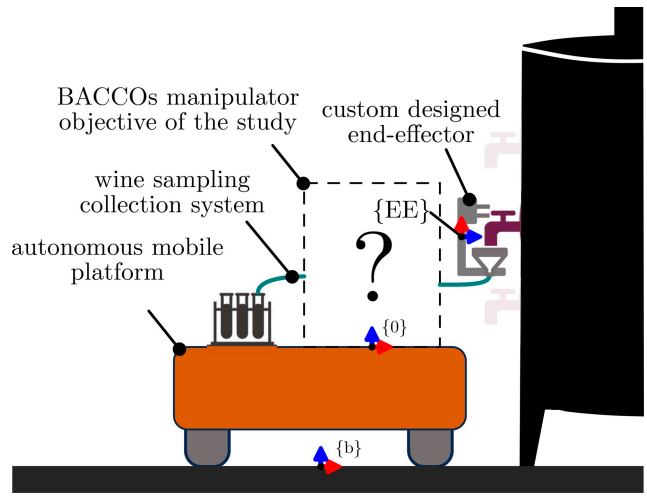

- implementation of two gravity compensation mechanisms. The cam-synthesis procedure originally proposed in Endo *et al.* (2010) has been reformulated into a more general and systematic framework, in which each step of the process is explicitly defined. This restructuring facilitates automated implementation through computational scripts, such as those developed in MATLAB, making the method more flexible, reproducible and readily applicable to a broader range of design scenarios; and
- experimental tests on a prototype of the low-mobility robot to validate the effectiveness of the proposed gravity compensation systems.

2. Requirements and functional design

The design process of BACCOs starts with the definition of its application requirements. The barrel taps are usually installed between 1.1 and 1.8 m above the ground. Usually, barrels are placed one after the other and are accessible from a corridor 2 m wide, as shown in Figure 2(a).

During the sampling activities, the robot moves along the corridors, stopping near the barrels. The robot then extracts samples from the left barrel, rotates of $\approx 180^{\circ}$ and extracts samples from the right one or vice versa. Ideally, the robot should move in the center of the corridors, but there may be obstacles on the ground that could cause it to move away from the center. For this reason, the manipulator should be designed considering a lateral reach (along the y-axis of the reference frame) in the range of 0.5 m up to 1.5 m. The base of the robotic arm is fixed to the mobile platform at a height of 0.40 m from the ground. Finally, the robotic arm should be able to compensate for possible pose errors of the mobile base, as shown in Figure 2(b). In particular, the base platform can have position and orientation errors with respect to the goal pose.

To address all these requirements, the robotic arm is designed as a four-degree-of-freedom (DOF) mechanism, as illustrated in Figure 3. The robotic arm has one prismatic joint P_1, one vertical revolute pair R_2 with the axis aligned with the

Downloaded from www.emerald.com/ir/article-pdf/doi/10.1108/IR-03-2026-0135/11890658/ir-03-2026-0135en.pdf by Politecnico di Torino user on 05 October 2026

Figure 2 (a) Workspace definition: corridor and barrel taps and (b) possible pose errors of the mobile base

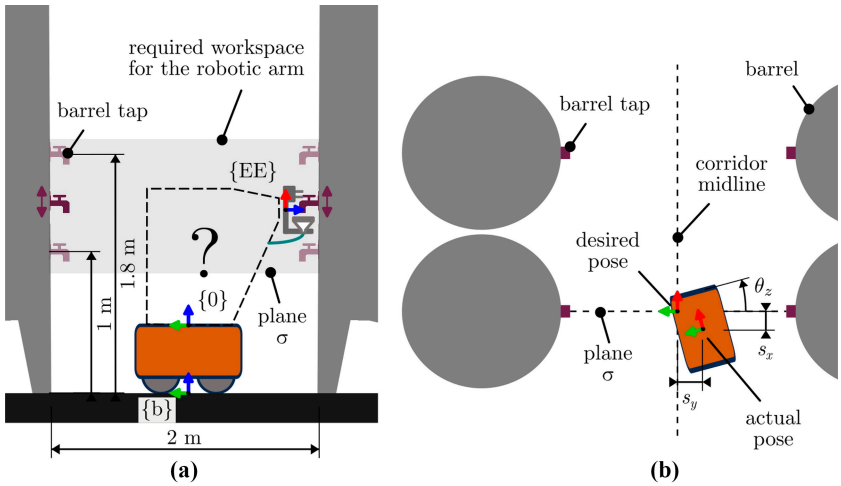

Figure 3 Robotic arm functional scheme: (a) 3D representation and (b) 2D representation with $q_2 = 0°$

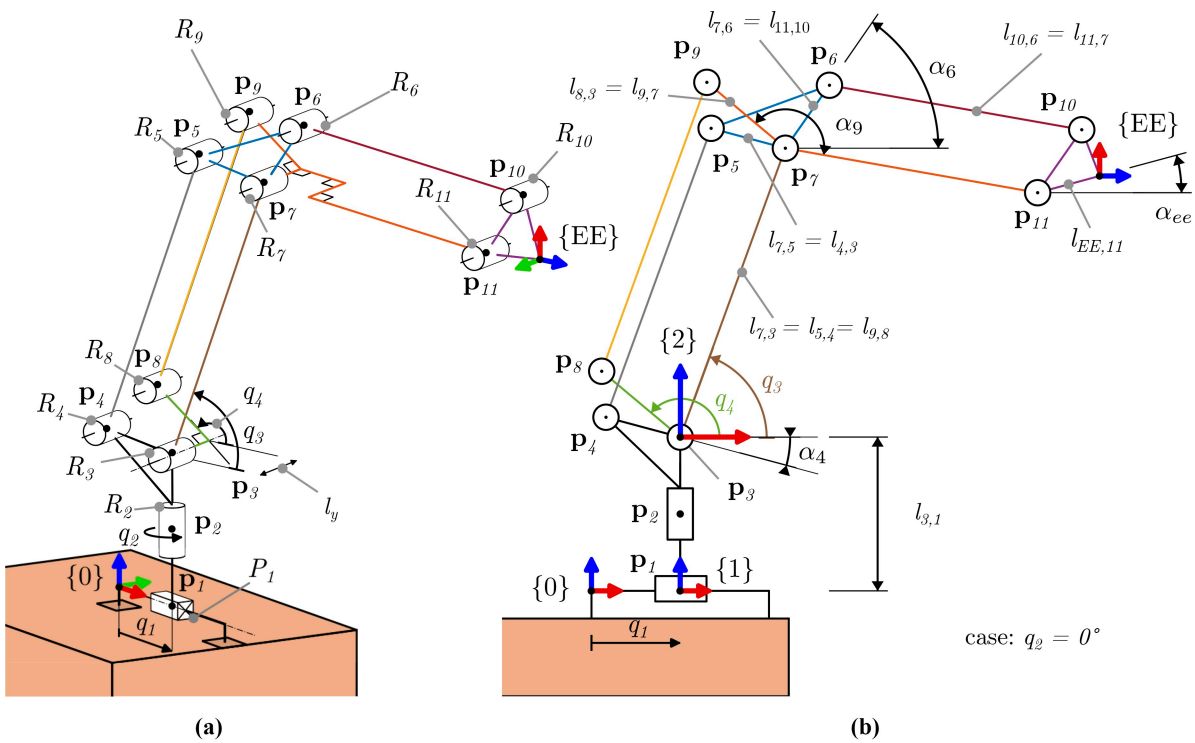

z-axis of $\{1\}$ (i.e. z_1) and nine revolute joints R_i ($i = 3, \ldots, 11$) with the axis parallel to y_2. The center of the joint R_j is $\mathbf{p}_j$ and the distance between two center points $\mathbf{p}_j$ and $\mathbf{p}_k$, measured in the XZ plane of $\{2\}$, is $l_{j,k} = l_{k,j}$. All revolute pairs have multiplicity of two except for R_3 and R_7 which have multiplicity of three.

Let us consider the subsystem composed of the planar mechanism R_i, $i = 3, \ldots, 11$. This part of the robotic arm is composed of nine links, that is, $N_{l,3,11} = 9$ (considering also the link that connects $\mathbf{p}_3$ and $\mathbf{p}_4$ whose pose is described by the reference frame $\{2\}$) and nine revolute joints (seven with multiplicity of two, that is, $N_{r_2,3,11} = 7$, and two with multiplicity of three $N_{j3,3,11} = 2$). Therefore, the number of DOF of this part of the system is:

$$F_{3,11} = 3(N_{l,3,11} - 1) - 2N_{j2,3,11} - 4N_{j3,3,11} = 2 \qquad (1)$$

If we consider the first part of the system, that is, up to the reference frame $\{2\}$ the system has two links, that is, $N_{l,1,2} = 2$ and two kinematic pairs (P_1 and R_2), that is, $N_{j,1,2} = 2$, that constraints five DOF in space. Therefore, the number of DOF of this part of the system is:

Downloaded from www.emerald.com/ir/article-pdf/doi/10.1108/IR-03-2026-0135/11890658/ir-03-2026-0135en.pdf by Politecnico di Torino user on 05 October 2026

$$F_{1,2} = 6(N_{l,1,2} - 1) - 5N_{j,1,2} = 2 \tag{2}$$

Thus, the total number of DOF is $F = F_{1,2} + F_{3,11} = 4$. Four DOF are the minimum number of DOF to achieve the desired sampling task. In fact, given the base platform positioning errors, P_1 and R_2 are needed to position the XZ plane of $\{EE\}$ on the σ plane [defined in Figure 2(b)] containing the barrel taps. Then the two DOF of the double-parallelogram planar mechanism are used to position $\{EE\}$ next to the barrel tap. The double-parallelogram planar mechanism is used because all the barrel taps are mounted with the same orientation; therefore, there is no need to change the orientation of the end effector. Given the kinematic structure of the planar manipulator, the two actuators can be installed on the link that connects $\mathbf{p}_3$ and $\mathbf{p}_4$.

The robotic arm motions can be controlled using the set of actuation variables $\mathbf{q} = \begin{bmatrix} q_1 & q_2 & q_3 & q_4 \end{bmatrix}^T$ as defined in Figure 3.

3. Kinematic model

This section presents the kinematic model of the robotic arm. The reference frame $\{0\}$ is fixed to the mobile platform. The orientation of $\{0\}$ is the same of $\{b\}$, that is, ${}^bR_0 = I_{3\times3}$, where $I_{3\times3}$ is the 3×3 identity matrix, while its origin is defined by the position vector ${}^b\mathbf{p}_0 = \begin{bmatrix} {}^bx_0 & {}^by_0 & {}^bz_0 \end{bmatrix}^T$. The pose of $\{1\}$ with respect to (*wrt* in the following) $\{0\}$ is computed as a pure translation q_1 along $x_0 = x_1$, while the pose of $\{2\}$ wrt $\{1\}$ is a rotation of q_2 around z_1. Therefore, the pose of $\{2\}$ wrt $\{0\}$ can be written as:

$$ {}^0T_2 = \begin{bmatrix} 1 & 0 & 0 & q_1 \\ 0 & 1 & 0 & 0 \\ 0 & 0 & 1 & 0 \\ 0 & 0 & 0 & 1 \end{bmatrix} \begin{bmatrix} c_{q_2} & -s_{q_2} & 0 & 0 \\ s_{q_2} & c_{q_2} & 0 & 0 \\ 0 & 0 & 1 & l_{3,1} \\ 0 & 0 & 0 & 1 \end{bmatrix} \tag{3}$$

where $c_{q_2} = \cos q_2$ and $s_{q_2} = \sin q_2$.

Once the linear and angular parameters are defined ($l_{j,k}$ distance between points $\mathbf{p}_j$ and $\mathbf{p}_k$ measured on the plane XZ of $\{2\}$, and angles α_i with $i = 4, 6, 9, ee$), the position of the revolute joints wrt $\{2\}$ can be evaluated as a function of the actuation angles q_3 and q_4 using equation (4):

$$\begin{cases} {}^2\mathbf{p}_4 = {}^2\mathbf{p}_3 + l_{4,3}\begin{bmatrix} c_{\pi-\alpha_4} & 0 & s_{\pi-\alpha_4} \end{bmatrix}^T & \text{(4a)} \\ {}^2\mathbf{p}_5 = {}^2\mathbf{p}_4 + l_{5,4}\begin{bmatrix} c_{q_3} & 0 & s_{q_3} \end{bmatrix}^T & \text{(4b)} \\ {}^2\mathbf{p}_6 = {}^2\mathbf{p}_7 + l_{7,6}\begin{bmatrix} c_{\alpha_6} & 0 & s_{\alpha_6} \end{bmatrix}^T & \text{(4c)} \\ {}^2\mathbf{p}_7 = {}^2\mathbf{p}_3 + l_{7,3}\begin{bmatrix} c_{q_3} & 0 & s_{q_3} \end{bmatrix}^T & \text{(4d)} \\ {}^2\mathbf{p}_8 = {}^2\mathbf{p}_3 + l_{8,3}\begin{bmatrix} c_{q_4} & 0 & s_{q_4} \end{bmatrix}^T + \begin{bmatrix} 0 & l_y & 0 \end{bmatrix}^T & \text{(4e)} \\ {}^2\mathbf{p}_9 = {}^2\mathbf{p}_8 + l_{9,8}\begin{bmatrix} c_{q_3} & 0 & s_{q_3} \end{bmatrix}^T + \begin{bmatrix} 0 & l_y & 0 \end{bmatrix}^T & \text{(4f)} \\ {}^2\mathbf{p}_{10} = {}^2\mathbf{p}_6 + l_{10,6}\begin{bmatrix} c_{q_4-\alpha_9} & 0 & s_{q_4-\alpha_9} \end{bmatrix}^T & \text{(4g)} \\ {}^2\mathbf{p}_{11} = {}^2\mathbf{p}_7 + l_{11,7}\begin{bmatrix} c_{q_4-\alpha_9} & 0 & s_{q_4-\alpha_9} \end{bmatrix}^T & \text{(4h)} \end{cases}$$

Given the kinematic properties of the double parallelogram, the orientation ${}^2R_{ee}$ of $\{EE\}$ wrt $\{2\}$ is constant, while its origin position can be computed as:

$$\begin{aligned} {}^2\mathbf{p}_{ee} &= {}^2\mathbf{p}_{11} + l_{EE,11}\begin{bmatrix} c_{\alpha_{ee}} & 0 & s_{\alpha_{ee}} \end{bmatrix}^T \\ &= \begin{bmatrix} l_{7,3}\, c_{q_3} + l_{11,7}\, c_{q_4-\alpha_9} + l_{EE,11}\, c_{\alpha_{ee}} \\ 0 \\ l_{7,3}\, s_{q_3} + l_{11,7}\, s_{q_4-\alpha_9} + l_{EE,11}\, s_{\alpha_{ee}} \end{bmatrix} \end{aligned} \tag{5}$$

Finally, the forward pose kinematics can be computed using equation (7). The pose of the end effector can be evaluated using equation (7) once the actuation vector $\mathbf{q}$ is defined:

$$\begin{aligned} {}^0T_{ee} = &\begin{bmatrix} 1 & 0 & 0 & q_1 \\ 0 & 1 & 0 & 0 \\ 0 & 0 & 1 & 0 \\ 0 & 0 & 0 & 1 \end{bmatrix} \begin{bmatrix} c_{q_2} & -s_{q_2} & 0 & 0 \\ s_{q_2} & c_{q_2} & 0 & 0 \\ 0 & 0 & 1 & l_{3,1} \\ 0 & 0 & 0 & 1 \end{bmatrix} \cdots \\ &\cdots \begin{bmatrix} 0 & 0 & 1 & l_{7,3}\, c_{q_3} + l_{11,7}\, c_{q_4-\alpha_9} + l_{EE,11}\, c_{\alpha_{ee}} \\ 0 & -1 & 0 & 0 \\ 1 & 0 & 0 & l_{7,3}\, s_{q_3} + l_{11,7}\, s_{q_4-\alpha_9} + l_{EE,11}\, s_{\alpha_{ee}} \\ 0 & 0 & 0 & 1 \end{bmatrix} \end{aligned} \tag{6}$$

$$\begin{aligned} {}^0T_{ee} &= \begin{bmatrix} {}^0R_{ee} & {}^0\mathbf{p}_{ee} \\ 0 \quad 0 & 0 \quad 1 \end{bmatrix} \\ &= \begin{bmatrix} 0 & s_{q_2} & c_{q_2} & q_1 + c_{q_2}(l_{7,3}\, c_{q_3} + l_{11,7}\, c_{q_4-\alpha_9} + l_{EE,11}\, c_{\alpha_{ee}}) \\ 0 & -c_{q_2} & s_{q_2} & s_{q_2}(l_{7,3}\, c_{q_3} + l_{11,7}\, c_{q_4-\alpha_9} + l_{EE,11}\, c_{\alpha_{ee}}) \\ 1 & 0 & 0 & l_{7,3}\, s_{q_3} + l_{11,7}\, s_{q_4-\alpha_9} + l_{EE,11}\, s_{\alpha_{ee}} \\ 0 & 0 & 0 & 1 \end{bmatrix} \end{aligned} \tag{7}$$

where ${}^0R_{ee}$ and ${}^0\mathbf{p}_{ee} = {}^0[x_{ee}, y_{ee}, z_{ee}]^T$ are the rotation matrix and the origin position of $\{EE\}$ wrt $\{0\}$.

To solve the inverse pose kinematic problem, it is useful to observe the system from above as represented in Figure 4. Just as a reminder, the inverse kinematics problem aims to determine the actuation variables, assuming as known the end-effector pose ${}^0T_{ee}$. Let us assume that the robotic system is provided with sensors (e.g. depth cameras, 3D lidars or similar) such that the barrel tap's pose wrt the robotic system is known.

If ${}^0R_{ee}$ is known, then the actuation variable q_2 can be evaluated as:

$$q_2 = \operatorname{atan2}\left({}^0R_{ee}(2,3), {}^0R_{ee}(1,3)\right) \tag{8}$$

where ${}^0R_{ee}(i,j)$ is the element (i,j) of the rotation matrix ${}^0R_{ee}$.

Once q_2 is known, the actuation variable q_1 can be computed as:

Downloaded from www.emerald.com/ir/article-pdf/doi/10.1108/IR-03-2026-0135/11890658/ir-03-2026-0135en.pdf by Politecnico di Torino user on 05 October 2026

Figure 4 Robotic system approaching a barrel tap: top view reference frames definition

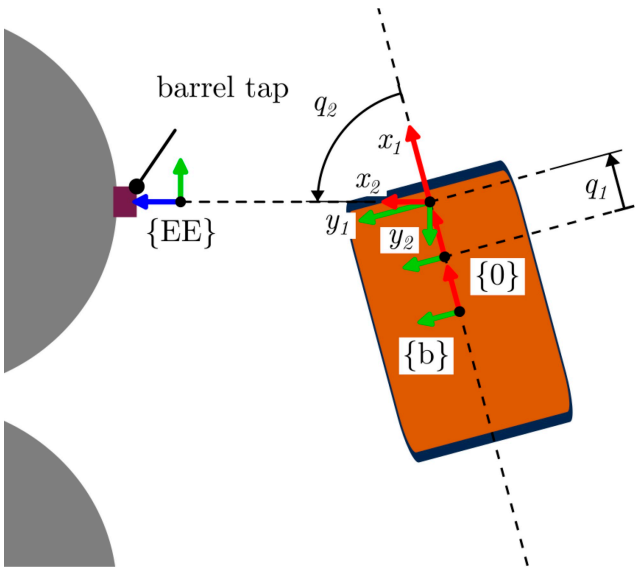

$$q_1 = \begin{cases} 0, & \text{if } q_2 = 0 + k\pi, \quad k \in \mathbb{Z}, \quad (9a) \\ {}^0x_{ee}, & \text{if } q_2 = \frac{\pi}{2} + k\pi, \quad k \in \mathbb{Z}, \quad (9b) \\ {}^0x_{ee} - \frac{{}^0y_{ee}}{\tan(q_2)}, & \text{otherwise} \quad (9c) \end{cases}$$

With q_1 and q_2, the transformation matrix ${}^0T_2$ of $\{2\}$ wrt $\{0\}$ can be computed using equation (3) and, then, the transformation matrix ${}^2T_{ee}$ can be evaluated as ${}^2T_{ee} = {}^2T_0\,{}^0T_{ee} = {}^0T_2^{-1}\,{}^0T_{ee}$. To solve the inverse kinematics, the system of equation (10) needs to be solved wrt the variables q_3 and q_4:

$$\begin{cases} l_{7,3}\, c_{q_3} + l_{11,7}\, c_{q_4-\alpha_9} = {}^2x_{ee} - l_{EE,11}\, c_{\alpha_{ee}} \\ l_{7,3}\, s_{q_3} + l_{11,7}\, s_{q_4-\alpha_9} = {}^2z_{ee} - l_{EE,11}\, s_{\alpha_{ee}} \end{cases} \iff$$

$$\iff \begin{cases} l_{7,3}\, c_{q_3} + l_{11,7}\, c_{q_4^*} = {}^2x^*_{ee} \\ l_{7,3}\, s_{q_3} + l_{11,7}\, s_{q_4^*} = {}^2z^*_{ee} \end{cases} \quad (10)$$

where $q_4^* = q_4 - \alpha_9$, ${}^2x^*_{ee} = {}^2x_{ee} - l_{EE,11}\, c_{\alpha_{ee}}$ and ${}^2z^*_{ee} = {}^2z_{ee} - l_{EE,11}\, s_{\alpha_{ee}}$. Solving equation (10) is equivalent to finding the angles q_3 and q_4^* in the geometric problem represented in Figure 5. First, the angle γ and the length l can be evaluated as:

$$\gamma = \text{atan2}\left({}^2z^*_{ee}, {}^2x^*_{ee}\right); \qquad l = \sqrt{{}^2x^{*\,2}_{ee} + {}^2z^{*\,2}_{ee}} \quad (11)$$

The angles α and β, restricted to lie in the interval $[0, \pi]$, can be determined using Carnot's theorem:

$$\alpha = \text{acos}\left(\frac{l^2 + l_{7,3}^2 - l_{11,7}^2}{2\, l\, l_{7,3}}\right); \qquad \beta = \text{acos}\left(\frac{l_{7,3}^2 + l_{11,7}^2 - l^2}{2\, l_{7,3}\, l_{11,7}}\right) \quad (12)$$

Figure 5 Geometric problem equivalent to the system of equation (10)

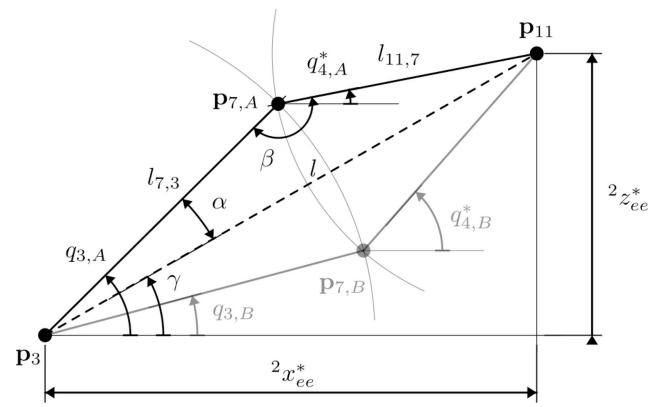

Thus, the two solutions of the inverse kinematic problem can be determined as:

$$\begin{cases} q_{3,A} = \gamma + \alpha \\ q^*_{4,A} = q_{3,A} + \beta - \pi \\ q_{4,A} = q_{3,A} + \beta - \pi + \alpha_9 \end{cases} \quad (13)$$

$$\begin{cases} q_{3,B} = \gamma - \alpha \\ q^*_{4,B} = q_{3,B} + \beta - \pi \\ q_{4,B} = q_{3,B} + \beta - \pi + \alpha_9 \end{cases} \quad (14)$$

In this manner, the pose of the robotic arm is fully defined. This kinematic model was used to carry out the dimensional synthesis of the robotic arm, too. However, the details of this process are omitted from this paper to maintain focus on the overall manipulator and balancing system. It is important to highlight that this process is iterative, considering both kinematic and design requirements. Table 1 summarizes all the geometric parameters of the robotic arm.

To access all potential locations of the barrel taps, the actuation variables q_3 and q_4 are defined within the following ranges: $q_3 \in [45°, 120°]$ and $q_4 \in [120°, 200°]$. A scaled representation of the functional scheme of the robotic arm is depicted in Figure 6. In addition, Figure 6(b) illustrates the domain of all possible barrel tap locations relative to the reference frame $\{2\}$ and the section in the XZ plane of $\{2\}$ of the actual robot workspace, considering the joint limits of q_3 and q_4.

4. Passive gravity compensation system

Under normal operating conditions, BACCOs is activated once the base platform reaches its target pose. During wine-sampling

Table 1 Linear and angular geometric parameters

Parameter	Value	Parameter	Value
$l_{3,1}$	0.354 m	$l_{7,3}$	1.142 m
$l_{7,5}$	0.15 m	$l_{8,3}$	0.18 m
$l_{11,7}$	0.901 m	$l_{EE,11}$	0.1 m
$l_{7,6}$	0.15 m	α_4	12°
α_6	55°	α_9	195°
α_{ee}	20°	–	–

Downloaded from www.emerald.com/ir/article-pdf/doi/10.1108/IR-03-2026-0135/11890658/ir-03-2026-0135en.pdf by Politecnico di Torino user on 05 October 2026

Figure 6 Robotic arm scaled functional scheme: (a) 3D representation and (b) 2D representation with $q_2 = 0°$. The gray rectangle represents the desired workspace, while the blue dots represent the actual workspace section on the *XZ* plane of $\{2\}$ considering q_3 and q_4 joint limits

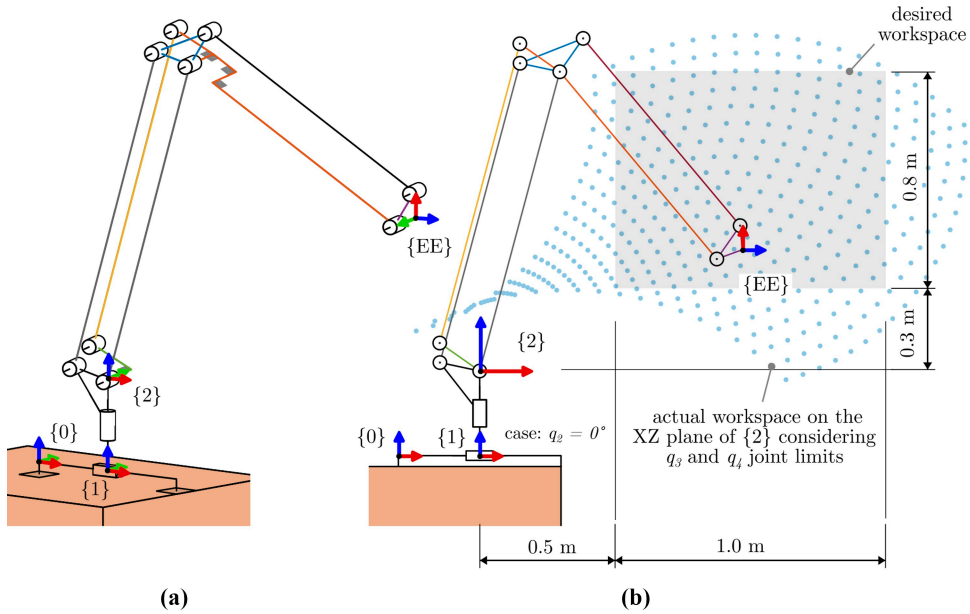

operations, the end effector remains stationary and is then retracted before moving to the next barrel. Given this type of use, a gravity compensation system can significantly enhance the energy efficiency of the robotic arm, as the actuators are primarily used to maintain a fixed configuration. Although the payload is relatively small (e.g. the end-effector weight is approximately 2.0 kg), the torques required to counteract gravity are significant due to the arm's extended reach. In addition, implementing a passive gravity compensation system can improve the safety of the mobile manipulator. For instance, if actuator power is unexpectedly lost, the robot will remain stationary rather than collapsing under its own weight.

This section presents two passive gravity compensation strategies to fully compensate the weight of the double-parallelogram planar mechanism within its operational workspace.

The first step in the design of a gravity compensation system is to derive a static model of the robotic arm to obtain the torque profile for each actuation joint to be compensated. Let us define $\mathbf{p}_{m_i}$ the position vector of the center of mass of the link i, whose mass is m_i. If we consider only the double-parallelogram planar mechanism, the velocity vector of each center of mass can be written as:

$$\dot{\mathbf{p}}_{m_i} = \frac{d}{dt}\mathbf{p}_{m_i} = \mathcal{J}_{m_i}(q_3, q_4)\begin{bmatrix}\dot{q}_3 & \dot{q}_4\end{bmatrix}^T \tag{15}$$

It follows that the actuator torque vector can be derived as:

$$\tau = \begin{bmatrix}\tau_3 & \tau_4\end{bmatrix}^T = \sum_i \mathcal{J}_{m_i}^T(q_3, q_4)\mathbf{F}_{m_i}; \tag{16}$$

where $\mathbf{F}_{m_i} = \begin{bmatrix}0 & 0 & -m_i g\end{bmatrix}^T$.

Figure 7 presents the functional scheme of the planar double-parallelogram mechanism with the center of gravity of each link. Analytically, the center of gravity positions wrt $\{2\}$ can be described using equation (17):

$$\begin{cases}
\mathbf{p}_{m_1} = \mathbf{p}_3 + l_{m_1}\begin{bmatrix}c_{q_3} & 0 & s_{q_3}\end{bmatrix}^T & (17a)\\
\mathbf{p}_{m_2} = \mathbf{p}_4 + l_{m_2}\begin{bmatrix}c_{q_3} & 0 & s_{q_3}\end{bmatrix}^T & (17b)\\
\mathbf{p}_{m_3} = \mathbf{p}_3 + l_{m_3}\begin{bmatrix}c_{q_4} & 0 & s_{q_4}\end{bmatrix}^T & (17c)\\
\mathbf{p}_{m_4} = \mathbf{p}_8 + l_{m_4}\begin{bmatrix}c_{q_3} & 0 & s_{q_3}\end{bmatrix}^T & (17d)\\
\mathbf{p}_{m_5} = \mathbf{p}_7 + l_{m_5}\begin{bmatrix}c_{\alpha_{m_5}} & 0 & s_{\alpha_{m_5}}\end{bmatrix}^T & (17e)\\
\mathbf{p}_{m_6} = \mathbf{p}_6 + l_{m_6}\begin{bmatrix}c_{q_4-\alpha_9} & 0 & s_{q_4-\alpha_9}\end{bmatrix}^T & (17f)\\
\mathbf{p}_{m_7} = \mathbf{p}_7 + l_{m_7}\begin{bmatrix}c_{q_4-\alpha_9+\alpha_{m_7}} & 0 & s_{q_4-\alpha_9+\alpha_{m_7}}\end{bmatrix}^T & (17g)\\
\mathbf{p}_{m_8} = \mathbf{p}_{11} + l_{m_8}\begin{bmatrix}c_{\alpha_6} & 0 & s_{\alpha_6}\end{bmatrix}^T & (17h)
\end{cases}$$

For the BACCOs manipulator, the torque vector to compensate for the gravity forces can be expressed as:

$$\tau = g\begin{bmatrix}(N_1 + N_2)c_{q_3}\\ N_3 c_{q_4} + N_4 c_{q_4-\alpha_9} + N_5 c_{q_4-\alpha_9+\alpha_{m_7}}\end{bmatrix} \tag{18}$$

where:

$$N_1 = l_{m_1}m_1 + l_{m_2}m_2 + l_{m_4}m_4$$
$$N_2 = l_{7,3}(m_5 + m_6 + m_7 + m_8 + m_{ee})$$
$$N_3 = l_{m_3}m_3 + l_{8,3}m_4$$
$$N_4 = l_{m_6}m_6 + l_{11,7}(m_8 + m_{ee})$$
$$N_5 = l_{m_7}m_7$$

Equation (18) proves that torques τ_3 and τ_4 only depend, respectively, on q_3 and q_4. It is therefore possible to design two

Downloaded from www.emerald.com/ir/article-pdf/doi/10.1108/IR-03-2026-0135/11890658/ir-03-2026-0135en.pdf by Politecnico di Torino user on 05 October 2026

Figure 7 Double-parallelogram planar mechanism functional scheme: definition of the centers of gravity of all links

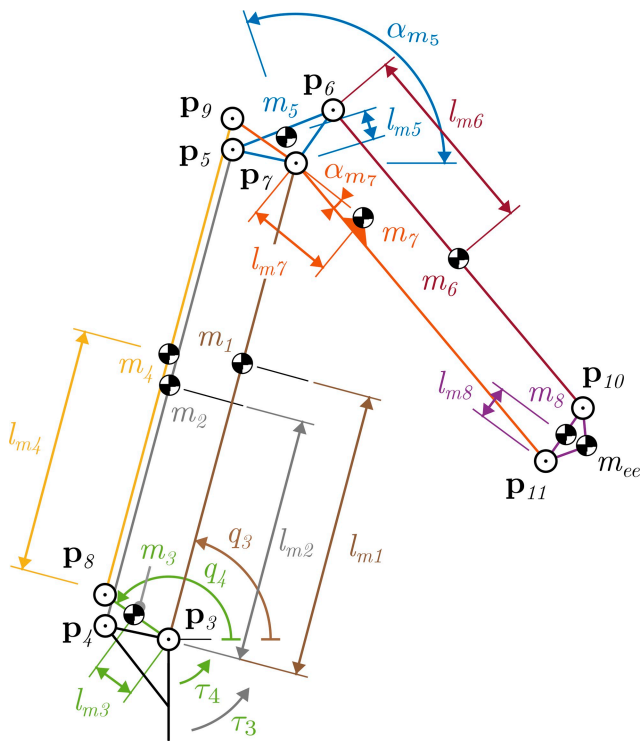

gravity compensation systems independently, one for each actuated joint. The masses m_i and the geometric parameters to locate the center of mass of each link are reported in Table 2. These parameters are evaluated using the mass estimator tool of SolidWorks software, used for the executive design of the system. With such parameters, it is possible to evaluate the trend of τ_3 and τ_4 as a function of q_3 and q_4, as shown in Figure 8.

Considering the torque profile to be generated by the balancing system, two different balancing methods are selected for the manipulator, namely, a spring-wire system for q_3 and a spring-wire-cam system for q_4. The functional scheme of the double parallelogram and the balancing systems are shown in Figure 9.

Figure 9(b) shows the functional details of the spring-wire balancing system used to obtain the gravity compensation

Table 2 Masses m_i and geometric parameters to locate the center of mass of each link

Parameter	Value	Parameter	Value
m_1	15.74 kg	m_2	0.48 kg
m_3	8.679 kg	m_4	2.24 kg
m_5	1.72 kg	m_6	1.07 kg
m_7	5.79 kg	m_8	0.20 kg
m_{ee}	2.0 kg	l_{m_1}	0.0.447 m
l_{m_2}	0.571 m	l_{m_3}	0.199 m
l_{m_4}	0.571 m	l_{m_5}	0.019 m
l_{m_6}	0.451 m	l_{m_7}	0.273 m
l_{m_8}	0.104 m	α_{m_5}	111.25°
α_{m_7}	3.37°	–	–

Figure 8 Torques (a) τ_3 and (b) τ_4 to compensate the gravity forces acting on the double-parallelogram mechanism

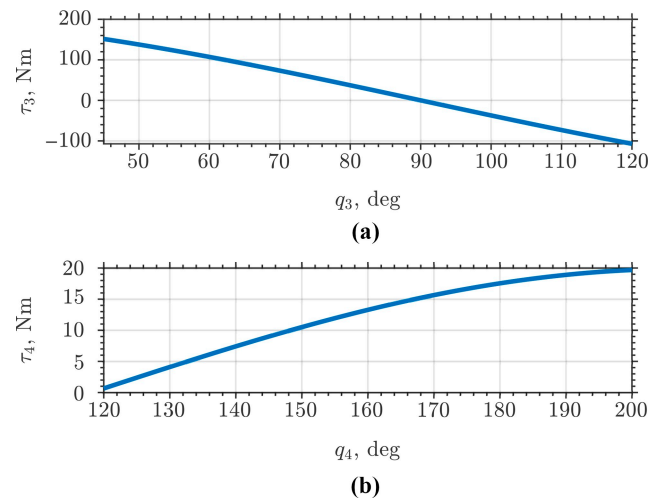

on q_3. A linear spring is attached, on one end, to the link that connects the revolute joints R_3 and R_7. On the other end, the linear spring is attached to a wire that passes through a passive pulley and that is fixed to link 2 (the link that connects the revolute joints R_3 and R_4) at the attachment point $\mathbf{p}_{k_{q_3,f}}$. If the pulley radius is small, the distance between points $\mathbf{p}_{k_{q_3,f}}$ and $\mathbf{p}_{k_{q_3,m}}$ can be evaluated from geometric considerations as:

$$\|\mathbf{p}_{k_{q_3,f}} - \mathbf{p}_{k_{q_3,m}}\| = \sqrt{l_{k_{q_3}}^2 |c_{q_3}|^2 + \left(l_{k_{q_3}} - l_{k_{q_3}} s_{q_3}\right)^2} \tag{19}$$

Suppose that the spring is adjusted so that its natural length is at $q_3 = \pi/2$. Thus, the spring force magnitude $F_{k_{q_3}}$, considered positive when the spring is under tension, can be determined as $F_{k_{q_3}} = k_{q_3}\|\mathbf{p}_{k_{q_3,f}} - \mathbf{p}_{k_{q_3,m}}\|$. This force acts on the link that connects the revolute joints R_3 and R_7, it is applied at point $\mathbf{p}_{k_{q_3,m}}$ and acts in the direction of the vector $(\mathbf{p}_{k_{q_3,f}} - \mathbf{p}_{k_{q_3,m}})$. Therefore, the balancing torque provided by the spring of stiffness k_{q_3} is:

$$\tau_{k_{q_3}} = \mathbf{p}_{k_{q_3,m}} \times \mathbf{F}_{k_{q_3}} = \mathbf{p}_{k_{q_3,m}} \times \left(k_{q_3}(\mathbf{p}_{k_{q_3,f}} - \mathbf{p}_{k_{q_3,m}})\right) = \begin{bmatrix} 0 \\ -k_{q_3} l_{k_{q_3}}^2 c_{q_3} \\ 0 \end{bmatrix} \tag{20}$$

To achieve the gravity compensation of this DOF, the torque provided by the balancing system must be equal to the torque τ_3 needed to compensate the gravity forces acting on the double-parallelogram mechanism. It should be noted that the torque τ_3 is defined as positive according to Figure 6. Therefore, to achieve the balancing effect, the stiffness of the spring k_{q_3} and the distance $l_{k_{q_3}}$ must be chosen such that equation (21) is verified:

$$k_{q_3} l_{k_{q_3}}^2 = g(N_1 + N_2) \tag{21}$$

Downloaded from www.emerald.com/ir/article-pdf/doi/10.1108/IR-03-2026-0135/11890658/ir-03-2026-0135en.pdf by Politecnico di Torino user on 05 October 2026

Figure 9 Functional schemes: (a) double-parallelogram planar mechanism with balancing systems and (b) details of the spring-wire balancing system used to obtain the gravity compensation on q_3

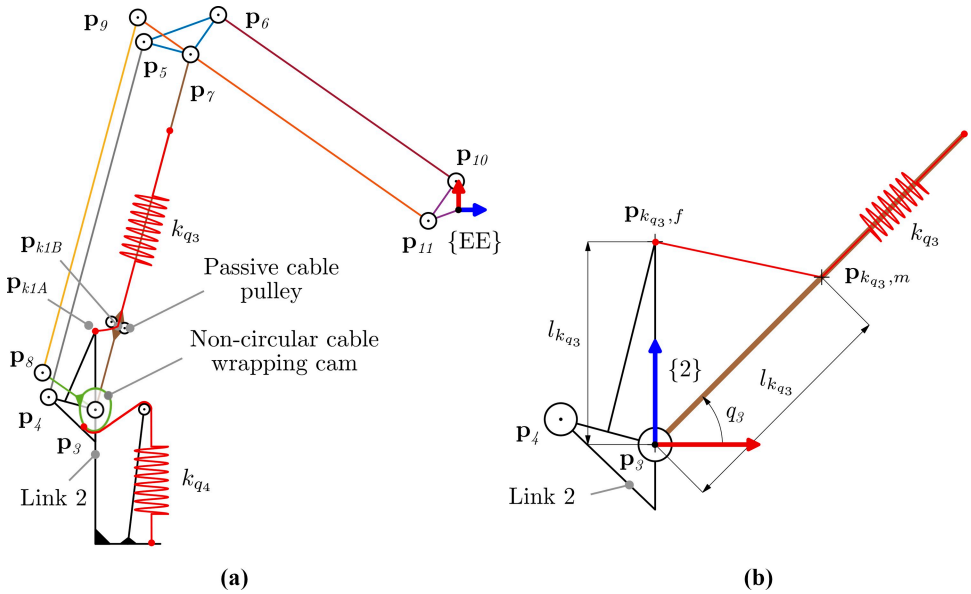

For example, given the mass, center of mass location of each link of BACCOs (Table 2) and a commercial spring with stiffness $k_{q_3} = 7.45$ kN/m, the attachment length must be $l_{k_{q_3}} = 0.185$ m.

Figure 10(a) shows the functional details of the spring-wire-cam balancing system used for the gravity compensation on the DOF q_4. A linear spring is attached to one end of link 2. On the other end, the linear spring is attached to a wire that passes through a passive pulley, and it is attached to a noncircular wrapping cam fixed to the link that connects the revolute joints R_3 and R_8. For the design of the wrapping pulley, it is useful to introduce a simpler nomenclature, as detailed in Figure 10(b).

Let us define the auxiliary angle α such that $\alpha = 0$ when $q_4 = q_{4,max}$ and $\alpha = q_{4,max} - q_{4,min}$ when $q_4 = q_{4,min}$. Therefore, $\alpha = q_{4,max} - q_4$ and $q_4 = q_{4,max} - \alpha$, for $q_4 \in [q_{4,min}, q_{4,max}]$. To design the cam, it is useful to consider the cam as fixed and the frame as rotating by an angle α in the opposite direction.

The cam synthesis problem is developed as an iterative method. On this topic, this work builds on existing literature by proposing a modified cam synthesis procedure based on Endo *et al.* (2010). The synthesis procedure originally proposed by Endo *et al.* (2010) has been reformulated into a more general and systematic framework, in which each step of the process is

Figure 10 Functional schemes: (a) spring-wire-cam system to balance the degree-of-freedom described by the variable q_4 and (b) graphic method for cam synthesis and nomenclature definition

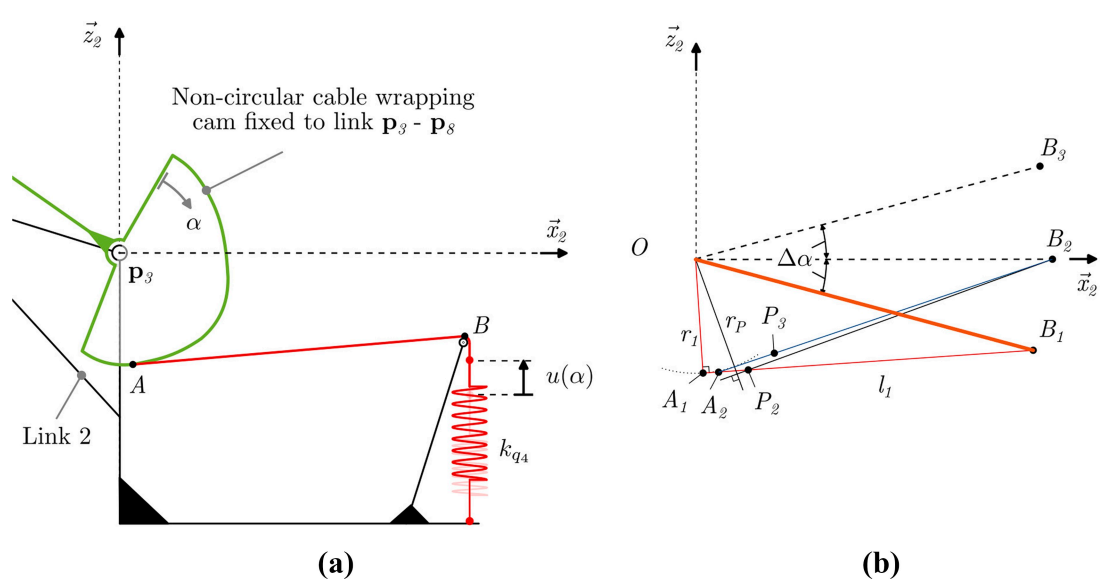

Downloaded from www.emerald.com/ir/article-pdf/doi/10.1108/IR-03-2026-0135/11890658/ir-03-2026-0135en.pdf by Politecnico di Torino user on 05 October 2026

explicitly defined. This restructuring facilitates automated implementation through computational scripts, such as those developed in MATLAB, making the method more flexible, reproducible and readily applicable to a broader range of design scenarios. At each interaction step i, the tangency point between the wire and the cam is called A_i, the tangency point between the wire and the passive pulley is called B_i and the point $\mathbf{p}_3$ is renamed O to simplify the nomenclature. The iterative procedure starts by setting $\alpha_1 = 0$ and arbitrarily choosing the radius r_1. First, the position of A_1 is computed such that $\overline{A_1B_1} \perp \overline{OA_1}$. Second, the length $l_1 = \|\mathbf{p}_{A_1} - \mathbf{p}_{B_1}\|$ and the initial spring force $F_1 = \tau_3(q_{4,max} - \alpha_1)/r_1$ are evaluated. Then, the spring stiffness k_{q_4} and the natural spring length u_n are chosen and the initial spring elongation u_1 is imposed such that $F_1 = (u_1 - u_n)k_{q_4} + F_n = \tau_4(q_{4,max} - \alpha_1)/r_1$, in which F_n is the preload at the natural length. Finally, the step increment $\Delta\alpha$ is chosen. Then, the iterative procedure starts by setting $i = 2$ and it proceeds with the following steps:

- Set $\alpha_i = \alpha_{i-1} + \Delta\alpha$;
- Place a point P_i on $\overline{A_{i-1}B_{i-1}}$, i.e., choose a value of a_i such that $\mathbf{p}_{P_i} = \mathbf{p}_{A_{i-1}} + a_i(\mathbf{p}_{A_{i-1}} - \mathbf{p}_{B_{i-1}})$;
- Evaluate the following quantities:
  - $l_i = l_{i-1} - (\|\mathbf{p}_{B_{i-1}} - \mathbf{p}_{P_i}\| - |\mathbf{p}_{B_i} - \mathbf{p}_{P_i}\|)$;
  - $F_i = (l_i - l_1)k_{q_4} + F_1$;
  - $r_i = \text{distance}(\text{line}(B_i, P_i), O)$, i.e., the distance between the line passing through points B_i and P_i and the origin O.
- Find the value of a_i such that $F_i r_i = \tau_4(q_{4,max} - \alpha_i)$ iterating points 2 and 3. If the correct value of a_i has been found, set $A_i = P_i$;
- Update $i = i + 1$, and iterate from point 1 to 5 until $\alpha_i \geq q_{4,max} - q_{4,min}$.

For the BACCOs manipulator, the following parameters have been used in the setup phase: spring stiffness $k_{q_4} = 2.77$ kN/m, spring natural length $u_n = 0.142$ m, spring preload $F_n = 68.74$ N; passive pulley B installed in position ${}^2\mathbf{p}_B = \begin{bmatrix} 0.2 & 0 & -0.14 \end{bmatrix}^T$ m; initial radius $r_1 = 0.08$ m. Considering the torque profile τ_4 represented in Figure 8, the resulting cam profile is shown in Figure 11.

Figure 11 Result of the cam synthesis procedure

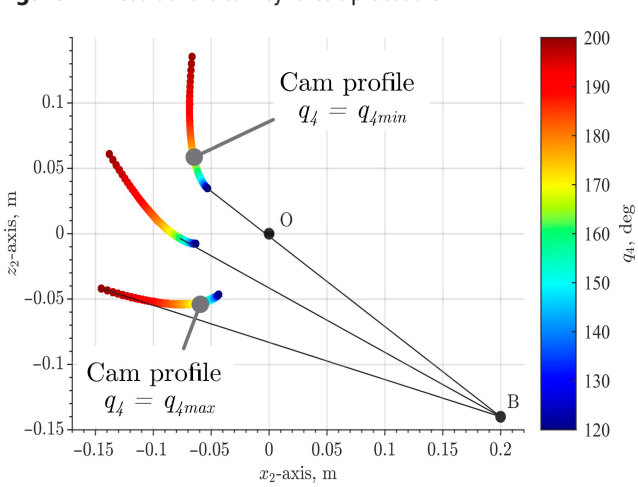

5. Executive design and prototype

Figure 12 shows three rendered views of the executive design of BACCO's prototype: Figure 12(a) shows a 3D view of the prototype, while Figure 12(b) and (c), shows, respectively, the spring-wire balancing system details for the DOF q_3 and the spring-wire-cam balancing system details for q_4. Moreover, Figure 12(b) and (c), shows the arrangement of springs, passive pulleys and wire routing for the two balancing systems.

Regarding the spring-wire balancing system adopted for q_3, two parallel springs are used to achieve the desired equivalent stiffness of $k_{q_3} = 7.45$ kN/m and the maximum elongation of the spring is 0.128 m. The wires are connected to the link that connects the revolute joints R_3 and R_4 at one end, while on the other side, the wires are connected to the free ends of the springs with eye bolts. To reduce the encumbrance of the balancing systems, the springs are mounted vertically and two passive pulleys are installed to obtain the wire routing shown in Figure 12(b).

Regarding the spring-wire-cam balancing system for q_4 a detailed view is shown in Figure 12(c). The cam profile, shown in blue, is attached to the link that connects the revolute joints R_3 and R_8. One end of the wire is fixed to the cam profile, while the other is fixed to the moving ring of the spring. The selected spring is a standard spring with stiffness $k_{q_4} = 2.77$ kN/m and maximum elongation of 0.280 m.

Particular attention in the executive design has been devoted to ensuring high bending stiffness. In particular, the links connecting R_3 to R_7 and R_7 to R_{11} are the most critical components in this regard. To improve the bending stiffness of these links, while keeping the weight low, these elements are designed from 1.5 mm thin steel profiles welded together. FEM analyses were performed iteratively during the executive design to ensure small deflection at the end-effector. FEM analysis with the final version of the prototype elongated to the limit of the workspace ($q_3 = 45^\circ$ and $q_4 = 200^\circ$) shows that, given an end-effector mass of 2.0 kg, the end-effector expected displacement resulting from the bending of the components is about 0.89 mm. Considering the total reach of the manipulator and the application, wine-sampling activities, this result has been considered acceptable.

After the executive design phase, a prototype was developed, as shown in Figure 13(a). Figure 13(b) and (c), illustrates the details of the two balancing systems. To validate the balancing performance and tune the control system, the robot was installed on a fixed platform, and 2.0 kg weights were attached to the end-effector flange to simulate the presence of the custom-made end effector. In future developments, BACCOs will be mounted on a mobile platform and equipped with the custom end effector for the wine-sampling operation.

The prototype is equipped with a motorized commercial linear guide by IGUS (model SLW-2080 TR18x4) to actuate the prismatic joint P_1, and three motors by ROBOTIS (Dynamixel XH540-W270-T) that drive the DOF q_2, q_3, and q_4 through timing belt transmissions (gear ratio $\tau_{motor}/\tau_{joint} = 1/5$). The motors are controlled by an electronic unit based on the OpenRB-150 Arduino-compatible embedded controller by ROBOTIS and powered by a supply that will be replaced with the onboard battery once the manipulator is integrated into the mobile platform.

Downloaded from www.emerald.com/ir/article-pdf/doi/10.1108/IR-03-2026-0135/11890658/ir-03-2026-0135en.pdf by Politecnico di Torino user on 05 October 2026

Figure 12 CAD view of BACCOs prototype without safety covers on the balancing systems: (a) 3D view; (b) spring-wire balancing system details; and (c) spring-wire-cam balancing system details

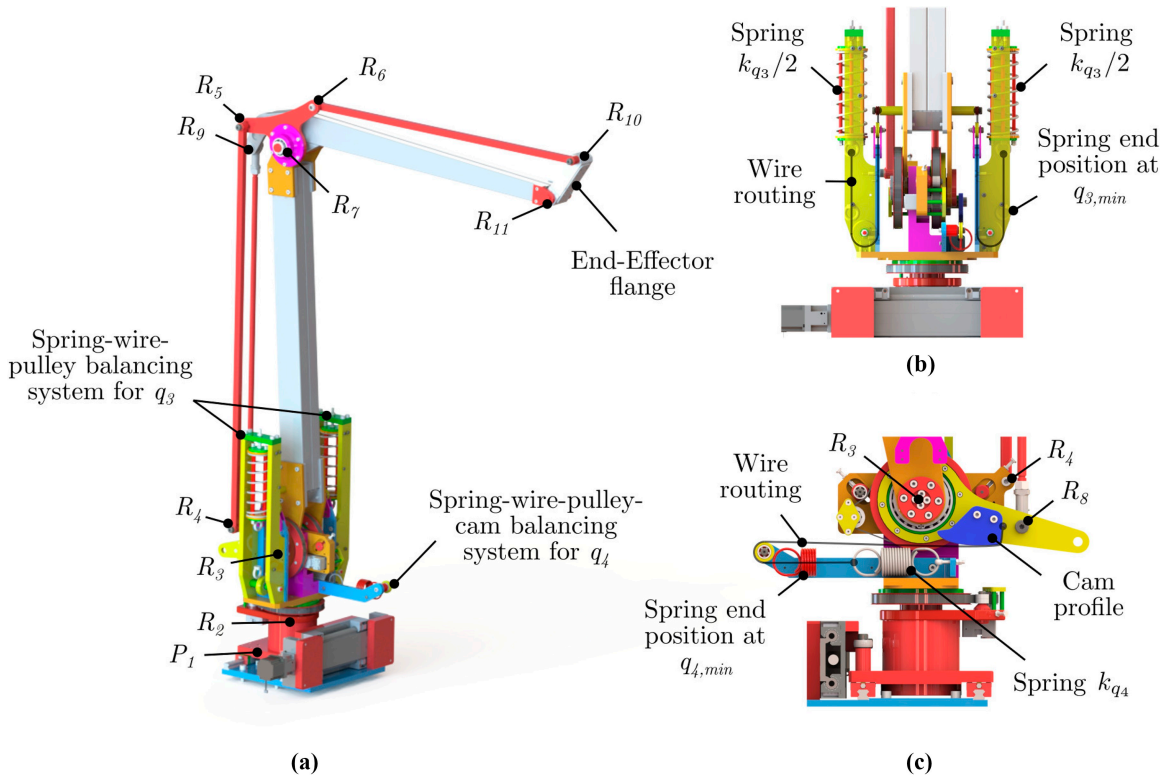

Figure 13 BACCOs prototype without safety covers on the balancing systems: (a) 3D view; (b) spring-wire balancing system; and (c) spring-wire-cam balancing system

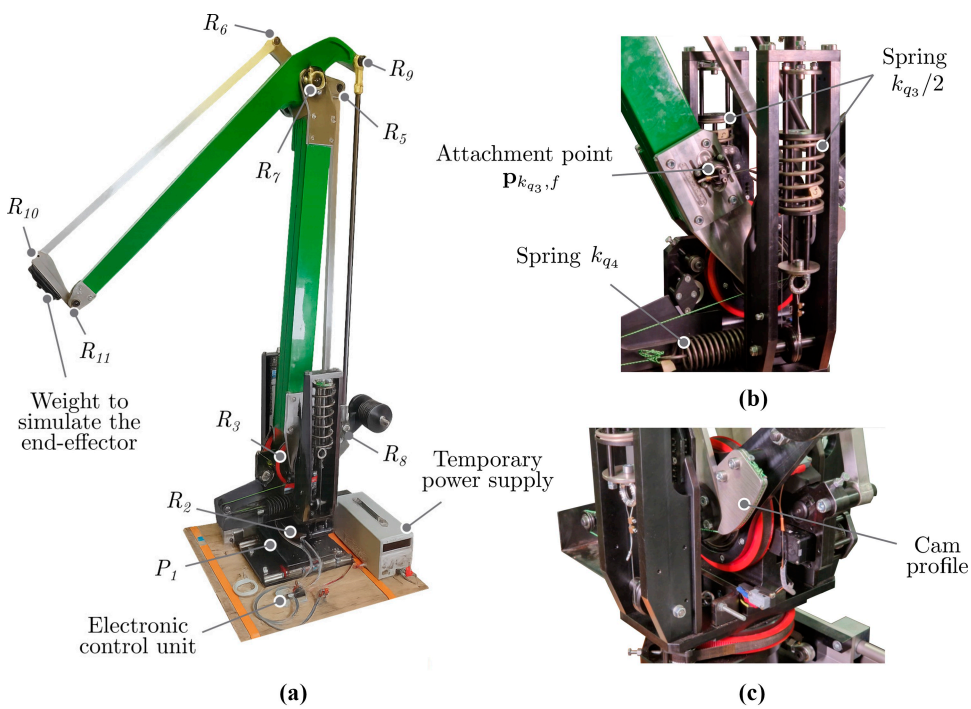

Downloaded from www.emerald.com/ir/article-pdf/doi/10.1108/IR-03-2026-0135/11890658/ir-03-2026-0135en.pdf by Politecnico di Torino user on 05 October 2026

6. Balancing system experimental validation

This section describes the experimental tests performed to validate the effectiveness of the balancing system, that is, to verify whether the mechanism is properly gravity compensated throughout its entire range of motion. Because the torque around q_3 and q_4 are decoupled, the DOF are tested independently.

During the experimental tests, the dynamixel motors driving joints q_3 and q_4 are controlled in position using the proprietary closed-loop extended position control mode. These motors are equipped with internal encoders and current sensors. The motor current–torque relationship is provided by the manufacturer (torque constant $k_\tau = 2.020$ Nm/A, for a current range of [0, 2.8] A). To experimentally determine the joint torques τ_3 and τ_4 required to statically balance the robotic arm, the internal encoders and current sensors of the motors were used.

Because the motors operate in extended position control mode and their multi-turn counters are reset at startup, an external limit switch is required to perform the homing procedure of the robotic arm. For this purpose, two limit switches are installed at $q_3^* = 120^\circ$ and $q_4^* = 200^\circ$.

The experimental routine was performed as follows:

- perform the homing procedure for joints q_3 and q_4;
- set $q_4 = 180^\circ$;
- span the range of motion of q_3 in 5° increments. At each position, stop the motion, wait for 1 s and measure the mean motor current over a 2.5 s interval. Repeat until the entire range of motion is evaluated;
- aet $q_3 = 90^\circ$; and
- span the range of motion of q_4 in 5° increments. At each position, stop the motion, wait for 1 s and measure the mean motor current over a 2.5 s interval. Repeat until the entire range of motion is evaluated.

The presented experimental routine has been performed 10 times and the results are represented graphically in Figure 14. In the left plots, both the theoretical joint torque needed without balancing system and the experimental data with the balancing system are reported. The plots on the right are a zoom of the measured joint torques: in gray the individual tests and in black the upper and lower bounds of the experimental data.

For joint q_3, the maximum absolute torque measured is 10.99 Nm, corresponding to 7.23% of the maximum theoretical torque required to balance the gravitational effects on q_3 (theoretical maximum: 152.00 Nm). For joint q_4, the maximum absolute torque measured is 0.49 Nm, which represents 2.30% of the maximum theoretical torque needed to counteract gravity on q_4 (theoretical maximum: 21.35 Nm).

It is important to underline that even if friction has been neglected in the static model of the robot, it is present in the actual prototype. Joint friction has a positive effect in reducing the torque needed to maintain a fixed configuration. For this reason, an additional test should have been performed to verify the effectiveness of gravity compensation systems without the effect of friction. In particular, it would have been interesting to reconstruct the torque profile experimentally without the balancing system. Unfortunately, the robot motors have been selected in the design phase to work with the gravity

Figure 14 Measured joint torques to balance the system within the range of motion of the robot, zoomed sections of the plots are highlighted with red lines

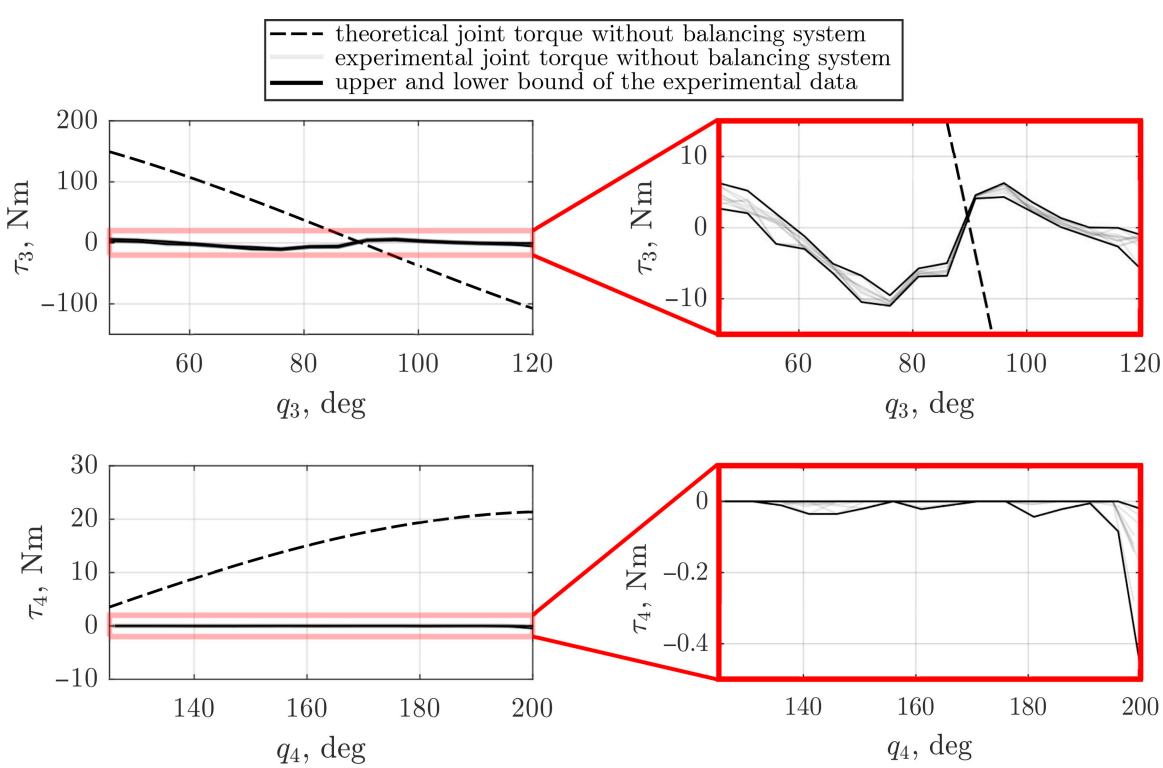

Downloaded from www.emerald.com/ir/article-pdf/doi/10.1108/IR-03-2026-0135/11890658/ir-03-2026-0135en.pdf by Politecnico di Torino user on 05 October 2026

compensation system; therefore, they are underpowered to actuate the robotic arm without it. During preliminary tests with the spring-wire-pulley balancing system disconnected, the motor acting on q_3 stalled outside the range $[75, 105]^\circ$. For $q_3 \in [75, 105]^\circ$, the absolute value of the theoretical joint torque is lower than 54.2 Nm. Considering the maximum motor torque 9.9 Nm and the transmission ratio $\tau_{motor}/\tau_{joint} = 1/5$, the difference between the theoretical stall and the experimental one is about 4.7 Nm (3.1% of the maximum theoretical torque τ_3). The presence of these differences indicates that, as expected, friction has an effect on the static behavior of the manipulator, but its impact is limited.

For these reasons, the experimental results can be interpreted as a solid validation of the effectiveness of the designed balancing system in reducing the torque required to statically support the robotic arm. This feature is particularly important for a robot such as BACCOs, which operates at relatively low speeds while maintaining a fixed end-effector position during wine-sampling operations.

7. Conclusion

In this work, a gravity-compensated 4-DOF manipulator specifically designed for automated wine sampling, named BACCOs, is proposed, developed and tested. The core element of the manipulator is a double-parallelogram mechanism, which functions as a positioner for a custom end effector dedicated to interacting with barrel taps to collect wine samples. This main mechanism is combined with a prismatic joint and a vertical revolute joint to achieve the minimum DOF required to reach the barrel taps while compensating for pose errors of the mobile platform. Subsequently, a kinematic analysis was performed, yielding closed-form expressions for both forward and inverse kinematics.

Due to the typical operational environment, the manipulator requires long links to reach the designated workspace. Furthermore, as the arm is mounted on a mobile platform, the entire system must be battery-powered. To address these constraints, passive gravity compensation was implemented through two independently tuned subsystems, reducing actuator size and enabling the robot to maintain its configuration with minimal power consumption. Specifically, a spring-wire system provides a nearly constant counter-torque for the q_3 joint across its workspace. For the q_4 joint, a cam profile was synthesized using an iterative geometric method, closely matching the nonlinear torque requirements of the double-parallelogram linkages via a spring-wire-cam mechanism. Mass properties obtained from SolidWorks were incorporated into the design process. Although not detailed in this study, the design process was iterative, as the executive design directly influences the balancing system and vice versa.

The executive design integrates these subsystems into a compact prototype, with springs and pulleys arranged to minimize the overall envelope. The spring-wire system for q_3 uses parallel springs to achieve the desired stiffness and elongation, while the spring-wire-cam system for q_4 uses a custom cam, routed wire and preload settings to accurately track the counter-torque curve. A prototype was built and programmed, and experimental tests were conducted to evaluate the effectiveness of the balancing systems. The results show that the maximum absolute residual torques required to statically balance the robotic arm for joints q_3 and q_4 are, respectively, 7.23% and 2.30% of the maximum theoretical torques needed to compensate for gravity.

The balancing system also enhances the safety of the robot. On one hand, in the event of an unexpected power loss, the system remains balanced and does not move. On the other hand, the use of the balancing system allows for smaller actuators, which reduces the forces generated by the motors in the event of a collision.

Future work will focus on integrating the manipulator with the mobile platform and the custom-designed end effector for wine sampling. The ultimate goal is to test the system under autonomous navigation and perform automated wine sample collection in experimental validation trials within operational winery environments.

References

Arakelian, V. (2016), "Gravity compensation in robotics", *Advanced Robotics*, Vol. 30 No. 2, pp. 79-96.

Arvin, F., Watson, S., Turgut, A.E., Espinosa, J., Krajník, T. and Lennox, B. (2018), "Perpetual robot swarm: long-term autonomy of mobile robots using on-the-fly inductive charging", *Journal of Intelligent & Robotic Systems*, Vol. 92 Nos 3-4, pp. 395-412.

Barnard, H., Dooley, A.N., Areshian, G., Gasparyan, B. and Faull, K.F. (2011), "Chemical evidence for wine production around 4000 BCE in the late chalcolithic near Eastern Highlands", *Journal of Archaeological Science*, Vol. 38 No. 5, pp. 977-984.

Chen, J., Chen, X. and Liu, S. (2023), "Trajectory planning of autonomous mobile robot using model predictive control in human-robot shared workspace", *in '2023 IEEE 3rd International Conference on Electronic Technology, Communication and Information (ICETCI)'*, pp. 462-467.

Colucci, G., Botta, A., Tagliavini, L., Cavallone, P., Baglieri, L. and Quaglia, G. (2022), "Kinematic modeling and motion planning of the mobile manipulator Agri.q for precision agriculture", *Machines (Basel)*, Vol. 10 No. 5, p. 321.

Endo, G., Yamada, H., Yajima, A., Ogata, M. and Hirose, S. (2010), "A passive weight compensation mechanism with a non-circular pulley and a spring", *in 2010 IEEE International Conference on Robotics and Automation*', *IEEE*, pp. 3843-3848.

Fragapane, G., de Koster, R., Sgarbossa, F. and Strandhagen, J.O. (2021), "Planning and control of autonomous mobile robots for intralogistics: literature review and research agenda", *European Journal of Operational Research*, Vol. 294 No. 2, pp. 405-426.

Gacovski, Z. and Gacovski, Z. (2011), *Mobile Robots: current Trends*, IntechOpen, Rijeka, Croatia.

Herder, J.L. (2001), "Energy-free systems. Theory, conception and design of statically", PhD thesis, Delft University of Technology.

Hong, S.H., Albia, B., Kyzer, T., Cornelius, J., Mark, E.R., Hall, A.J. and Wang, Y. (2024), "Artificial neural network-based model predictive visual servoing for mobile robots", *Robotica*, Vol. 42 No. 8, pp. 2825-2847.

Jokić, A., Petrović, M. and Miljković, Z. (2022), "Real-time mobile robot perception based on deep learning detection model", in Karabegović, I., Kovačević A. and Mandžuka, S.

Downloaded from www.emerald.com/ir/article-pdf/doi/10.1108/IR-03-2026-0135/11890658/ir-03-2026-0135en.pdf by Politecnico di Torino user on 05 October 2026

(Eds), '*New Technologies, Development and Application V*, ' Springer International Publishing, Cham, pp. 670-677.

Kececi, E.F. and Ceccarelli, M. (2015), *Mobile Robots for Dynamic Environments*, ASME Press.

Kilic, M., Yazicioglu, Y. and Kurtulus, D.F. (2012), "Synthesis of a torsional spring mechanism with mechanically adjustable stiffness using wrapping cams", *Mechanism and Machine Theory*, Vol. 57, pp. 27-39.

Lowen, G.G., Tepper, F.R. and Berkof, R.S. (1983), "Balancing of linkages—an update", *Mechanism and Machine Theory*, Vol. 18 No. 3, pp. 213-220.

Mashayekhi, A., Nahvi, A., Yazdani, M., Mohammadi Moghadam, M., Arbabtafti, M. and Norouzi, M. (2014), "VirSense: a novel haptic device with fixed-base motors and a gravity compensation system", *Industrial Robot: An International Journal*, Vol. 41 No. 1, pp. 37-49, doi: 10.1108/IR-02-2013-328.

Millon, M. (2013), *Wine: A Global History*, Reaktion Books.

Pao, J.C., Banglos, C.A.G., Salaan, C.J.O. and Guirnaldo, S.A. (2022), "Simulation and strength analysis of flippable mobile ground robot for volcano exploration and monitoring application", *in 2022 IEEE 14th International Conference on Humanoid, Nanotechnology, Information Technology, Communication and Control, Environment, and Management (HNICEM)*', *IEEE*, pp. 1-6.

Payá, L., Payá, L. and Reinoso Garcia, O. (2020), *Mobile Robots Navigation*, Multidisciplinary Digital Publishing Institute, Basel, Switzerland.

Quaglia, G., Tagliavini, L., Colucci, G., Vorfi, A., Botta, A. and Baglieri, L. (2022), "Design and prototyping of an interchangeable and underactuated tool for automatic harvesting", *Robotics (Basel)*, Vol. 11 No. 6, p. 145.

Te Riele, F.L. and Herder, J.L. (2001), "Perfect static balance with normal springs", in *International Design Engineering Technical Conferences and Computers and Information in Engineering Conference*, *American Society of Mechanical Engineers*, pp. 571-578, available at: https://asmedigitalcollection.asme.org/IDETC-CIE/proceedings-abstract/IDETC-CIE2001/571/1090754

Siegwart, R., Nourbakhsh, I.R. and Scaramuzza, D. (2011), "Introduction to autonomous mobile robots/Roland Siegwart, Illah R", *Nourbakhsh, Davide Scaramuzza*, 2nd Ed., MIT Press, Cambridge (Mass).

Watanabe, A., Mitsuhashi, T., Okugawa, M., Ogane, K., Kimura, T., Kinugasa, T. and Ohtsubo, Y. (2024), "Ground adaptability of crawler mobile robots with Sub-crawler rotary joint compliance", *Journal of Robotics and Mechatronics*, Vol. 36 No. 3, pp. 732-745.

Xiao, X., Liu, B., Warnell, G. and Stone, P. (2022), "Motion planning and control for mobile robot navigation using machine learning: a survey", *Autonomous Robots*, Vol. 46 No. 5, pp. 569-597.

Yin, Z. (2014), "Serial and parallel robotics: energy saving systems and rehabilitation devices", PhD thesis, Politecnico di Torino.

Corresponding author

Luigi Tagliavini can be contacted at: luigi.tagliavini@polito.it

For instructions on how to order reprints of this article, please visit our website:
www.emeraldgrouppublishing.com/licensing/reprints.htm
Or contact us for further details: **permissions@emeraldinsight.com**

Downloaded from www.emerald.com/ir/article-pdf/doi/10.1108/IR-03-2026-0135/11890658/ir-03-2026-0135en.pdf by Politecnico di Torino user on 05 October 2026